Mesoscopic stability and sedimentation waves in settling periodic arrays

B. U. Felderhof*
Institut für Theoretische Physik A, RWTH Aachen Templergraben 55, 52056 Aachen, Germany
(Received 6 June 2003; published 11 November 2003)

The stability of a periodic array of particles settling in a viscous incompressible fluid under the influence of gravity is investigated in the framework of the point sedimentation model. The simple cubic array is unstable, but the body-centered and face-centered cubic arrays with gravity directed along one of the crystal axes are mesoscopically stable, i.e., they are stable except for very long wavelength in a certain domain of directions of the wave vector. In such mesoscopically stable arrays the instability is suppressed in periodic boundary conditions for systems smaller than a maximum size. In a stable finite system the particles perform small motions about the positions of the regular array, and sedimentation waves propagate through the system.

DOI: 10.1103/PhysRevE.68.051402 PACS number(s): 82.70.Dd, 47.15.Gf, 47.15.Pn, 83.10.Pp

I. INTRODUCTION

The average velocity of particles and fluid in a suspension of spheres settling in a viscous incompressible fluid has been studied in detail for both ordered arrays and disordered systems of particles. In a pioneering work Hasimoto [1] showed how to construct and interpret a solution of the steady state Stokes equations for infinite regular arrays. At low particle volume fraction ϕ the sedimentation velocity decreases from the Stokes value in proportion to $\phi^{1/3}$, and it steadily decreases further at higher volume fraction [1–3]. Batchelor [4] first showed that for disordered systems, with complete neglect of correlations in particle positions, the sedimentation velocity decreases rapidly with volume fraction, in proportion to $1-6.55\phi$. Calculations to higher order in volume fraction [5,6] suggest that the sedimentation velocity of a disordered system vanishes at a volume fraction of about 20%. The lack of experimental evidence for this phenomenon indicates that the assumption of a disordered hard sphere distribution is not correct [7]. The determination of the statistical distribution of a disordered sedimenting suspension and the calculation of the corresponding sedimentation velocity is still an open problem [8–10].

The calculation of the variance of particle velocity fluctuations leads to worse difficulties. Even for dilute systems, where the point approximation is reliable, the variance diverges with the size of the system if the particle distribution is random [11,12]. It has been suggested that a form of hydrodynamic screening is necessary to keep the variance finite [13]. The divergence with the size of the system is not seen in experiment [14]. Several theoretical explanations have been advanced [15–19].

In the following, we study the stability of sedimenting periodic arrays in point approximation. The point approximation applies to sufficiently dilute systems. Crowley has shown that linear and planar regular arrays are not stable [20,21], but he reserved judgment on three-dimensional arrays. Three-dimensional regular arrays are reputed to be unstable [10,22–24]. We find that such arrays are mesoscopically stable for suitable crystal structure and orientation with respect to the direction of gravity, i.e., they are stable except for very long wavelength of the disturbance. Mesoscopically stable arrays are unstable on a macroscopic length scale, but the instability is suppressed in periodic boundary conditions for systems smaller than a maximum size that is many times larger than the size of a unit cell of the array.

II. PERTURBATION OF HASIMOTO'S SOLUTION

We consider a system of identical spherical particles of radius a immersed in a viscous incompressible fluid with shear viscosity η. In Hasimoto's solution of the steady state Stokes equations the particle centers are located at a regular array of positions

$$\boldsymbol{R}_{\boldsymbol{n}}=n_1\boldsymbol{a}_1+n_2\boldsymbol{a}_2+n_3\boldsymbol{a}_3 \quad (n_1,n_2,n_3=0,\pm1,\pm2,\ldots), \tag{1}$$

where $\boldsymbol{a}_1,\boldsymbol{a}_2$, and $\boldsymbol{a}_3$ are the basic vectors determining the unit cell of the array. The fluid velocity $\boldsymbol{v}$ and pressure p satisfy the linear Navier-Stokes equations

$$\eta\nabla^2\boldsymbol{v}-\boldsymbol{\nabla}p=-\boldsymbol{F}(\boldsymbol{r}), \quad \boldsymbol{\nabla}\cdot\boldsymbol{v}=0, \tag{2}$$

where $\boldsymbol{F}(\boldsymbol{r})$ is the force density acting on the fluid. In point approximation the force density is given by

$$\boldsymbol{F}(\boldsymbol{r})=\sum_{\boldsymbol{n}}\boldsymbol{K}\delta(\boldsymbol{r}-\boldsymbol{R}_{\boldsymbol{n}}), \tag{3}$$

where $\boldsymbol{K}$ is the force of gravity acting on each particle. Again in point approximation Hasimoto's solution for fluid velocity and pressure takes the form

$$\begin{aligned}\boldsymbol{v}_H(\boldsymbol{r})&=-\boldsymbol{U}+\mathsf{T}_H(\boldsymbol{r})\cdot\boldsymbol{K},\\ p_H(\boldsymbol{r})&=\frac{1}{v_c}\boldsymbol{K}\cdot\boldsymbol{r}+\mathsf{Q}_H(\boldsymbol{r})\cdot\boldsymbol{K},\end{aligned} \tag{4}$$

where v_c is the volume of the unit cell and the Green functions $\mathsf{T}_H(\boldsymbol{r})$ and $\mathsf{Q}_H(\boldsymbol{r})$ have the periodicity of the lattice. The Hasimoto tensor $\mathsf{T}_H(\boldsymbol{r})$ has the property

*Electronic address: ufelder@physik.rwth-aachen.de

$$\int_{v_c} \mathsf{T}_H(\boldsymbol{r})d\boldsymbol{r}=0, \tag{5}$$

so that in point approximation $-\boldsymbol{U}$ is the mean fluid velocity related to the force $\boldsymbol{K}$ by $\boldsymbol{K}=\zeta\boldsymbol{U}$, where $\zeta=6\pi\eta a$ is the friction coefficient of a single particle. Hasimoto has considered corrections due to finite particle size. His calculations were complemented by Zick and Homsy [2] and by Sangani and Acrivos [3].

In Hasimoto's solution the regular array of particles is at rest. Next we consider a situation where the particles are displaced from the regular positions. The actual position of the particle corresponding to lattice site $\boldsymbol{R_n}$ will be

$$\boldsymbol{r_n}=\boldsymbol{R_n}+\boldsymbol{s_n}, \tag{6}$$

with displacement vector $\boldsymbol{s_n}$. The fluid velocity and pressure are modified to

$$\begin{aligned}\boldsymbol{v}(\boldsymbol{r})&=\boldsymbol{v}_H(\boldsymbol{r})+\sum_{\boldsymbol{n}}\,[\mathsf{T}(\boldsymbol{r}-\boldsymbol{r_n})-\mathsf{T}(\boldsymbol{r}-\boldsymbol{R_n})]\cdot\boldsymbol{K},\\ p(\boldsymbol{r})&=p_H(\boldsymbol{r})+\sum_{\boldsymbol{n}}\,[\mathsf{Q}(\boldsymbol{r}-\boldsymbol{r_n})-\mathsf{Q}(\boldsymbol{r}-\boldsymbol{R_n})]\cdot\boldsymbol{K},\end{aligned} \tag{7}$$

with Oseen tensor and vector

$$\mathsf{T}(\boldsymbol{r})=\frac{1}{8\pi\eta}\frac{\mathbf{1}+\hat{\boldsymbol{r}}\hat{\boldsymbol{r}}}{r},\quad \mathsf{Q}(\boldsymbol{r})=\frac{\hat{\boldsymbol{r}}}{4\pi r^2}. \tag{8}$$

The sums converge if the displacements decay sufficiently fast with distance from the origin. The particle velocity $\boldsymbol{u_n}$ and the force $\boldsymbol{K}$ are related by

$$\boldsymbol{K}=\zeta(\boldsymbol{u_n}-\boldsymbol{v}_{\boldsymbol{n}}'), \tag{9}$$

where $\boldsymbol{v}_{\boldsymbol{n}}'$ is the velocity field incident on particle $\boldsymbol{n}$. To first order in the displacements,

$$\frac{d\boldsymbol{s_n}}{dt}=\sum_{\boldsymbol{m}\neq\boldsymbol{n}}(\boldsymbol{s_n}-\boldsymbol{s_m})\cdot\boldsymbol{\nabla}\mathsf{T}(\boldsymbol{r})|_{\boldsymbol{R_n}-\boldsymbol{R_m}}\cdot\boldsymbol{K}. \tag{10}$$

By symmetry the first term does not contribute, so that we can write

$$\frac{d\boldsymbol{s_n}}{dt}=-\frac{K}{8\pi\eta}\sum_{\boldsymbol{m}\neq\boldsymbol{n}}\mathsf{F}_{\boldsymbol{nm}}\cdot\boldsymbol{s_m}, \tag{11}$$

where the tensor $\mathsf{F}_{\boldsymbol{nm}}=\mathsf{F}(\boldsymbol{R_n}-\boldsymbol{R_m})$ is given by

$$\tilde{\mathsf{F}}(\boldsymbol{R})=\frac{\partial}{\partial\boldsymbol{R}}\hat{\mathsf{T}}(\boldsymbol{R})\cdot\hat{\boldsymbol{K}}, \tag{12}$$

with the definitions $\hat{\mathsf{T}}(\boldsymbol{R})=8\pi\eta\mathsf{T}(\boldsymbol{R})$ and $\hat{\boldsymbol{K}}=\boldsymbol{K}/K$. The tensor $\mathsf{F}(\boldsymbol{R})$ has Cartesian components

$$\mathsf{F}_{\alpha\beta}(\boldsymbol{R})=\delta_{\alpha\beta}\frac{\hat{\boldsymbol{K}}\cdot\boldsymbol{R}}{R^3}-\hat{K}_\alpha\frac{R_\beta}{R^3}+\hat{K}_\beta\frac{R_\alpha}{R^3}-3\frac{\hat{\boldsymbol{K}}\cdot\boldsymbol{R}}{R^5}R_\alpha R_\beta. \tag{13}$$

We note that the tensor is traceless,

$$\mathrm{Tr}\mathsf{F}(\boldsymbol{R})=0, \tag{14}$$

since $\boldsymbol{\nabla}\cdot\mathsf{T}(\boldsymbol{r})=0$. In the following section we study the solution of the linear equations of motion (11).

III. LINEAR EQUATIONS OF MOTION

Crowley's results on one- and two-dimensional arrays suggest that the regular arrays studied by Hasimoto are not stable if the particles are free to move. In this section we study stability by use of the linear equations of motion (11). The periodicity of the regular array suggests plane wave solutions. Substituting a plane wave of the form

$$\boldsymbol{s_n}(t)=\boldsymbol{u_k}\exp(i\boldsymbol{k}\cdot\boldsymbol{R_n}-i\omega t), \tag{15}$$

we obtain

$$\omega_K\hat{\mathsf{F}}(\boldsymbol{k})\cdot\boldsymbol{u_k}=\omega(\boldsymbol{k})\boldsymbol{u_k}, \tag{16}$$

with characteristic frequency

$$\omega_K=\frac{K}{8\pi\eta d^2}. \tag{17}$$

The real-valued dimensionless tensor $\hat{\mathsf{F}}(\boldsymbol{k})$ is given by the lattice sum

$$\hat{\mathsf{F}}(\boldsymbol{k})=id^2{\sum_{\boldsymbol{n}}}'\,\mathsf{F}(\boldsymbol{R_n})\exp(i\boldsymbol{k}\cdot\boldsymbol{R_n}). \tag{18}$$

Here we have used the antisymmetry under inversion, $\mathsf{F}(-\boldsymbol{R})=-\mathsf{F}(\boldsymbol{R})$. Upon substitution of Eq. (13) we can evaluate the lattice sum by the method of Ewald summation [25]. For $\boldsymbol{k}\neq\boldsymbol{0}$ the lattice sum is absolutely convergent, but the sum diverges in the limit $\boldsymbol{k}\to\boldsymbol{0}$. It turns out that the eigenfrequencies remain finite.

In the notation of Nijboer and de Wette [25] we consider the lattice sum

$$S'\left(\boldsymbol{R}\left|\frac{\boldsymbol{k}}{2\pi},p\right.\right)={\sum_{\boldsymbol{n}}}'\,\frac{\exp(i\boldsymbol{k}\cdot\boldsymbol{R_n})}{|\boldsymbol{R}-\boldsymbol{R_n}|^{2p}}. \tag{19}$$

The tensor $\hat{\mathsf{F}}(\boldsymbol{k})$ can be expressed as

$$\hat{\mathsf{F}}(\boldsymbol{k})=X(\boldsymbol{k})\mathbf{1}+\mathsf{Y}(\boldsymbol{k})+\mathsf{Z}(\boldsymbol{k}), \tag{20}$$

where $\mathsf{Y}(\boldsymbol{k})$ is antisymmetric and $\mathsf{Z}(\boldsymbol{k})$ is symmetric. The scalar $X(\boldsymbol{k})$ is given by

$$X(\boldsymbol{k}) = d^2 \hat{\boldsymbol{K}} \cdot \frac{\partial}{\partial \boldsymbol{k}} S'\left(\boldsymbol{0} \left| \frac{\boldsymbol{k}}{2\pi}, \frac{3}{2}\right.\right). \tag{21}$$

By inversion symmetry of the array the sum $S'(\boldsymbol{0}|(\boldsymbol{k}/2\pi),p)$ is real for real p and symmetric under inversion $\boldsymbol{k} \to -\boldsymbol{k}$. The antisymmetric tensor $\mathbf{Y}(\boldsymbol{k})$ has components

$$Y_{\alpha\beta}(\boldsymbol{k}) = -d^2 \left(\hat{K}_\alpha \frac{\partial}{\partial k_\beta} - \hat{K}_\beta \frac{\partial}{\partial k_\alpha} \right) S'\left(\boldsymbol{0} \left| \frac{\boldsymbol{k}}{2\pi}, \frac{3}{2}\right.\right) \tag{22}$$

and the symmetric tensor $\mathbf{Z}(\boldsymbol{k})$ is given by

$$\mathbf{Z}(\boldsymbol{k}) = 3d^2 \hat{\boldsymbol{K}} \cdot \frac{\partial^3}{\partial \boldsymbol{k} \partial \boldsymbol{k} \partial \boldsymbol{k}} S'\left(\boldsymbol{0} \left| \frac{\boldsymbol{k}}{2\pi}, \frac{5}{2}\right.\right). \tag{23}$$

The tensor $\hat{\mathbf{F}}(\boldsymbol{k})$ depends only on crystalline structure and on the direction of the force. For each wave vector $\boldsymbol{k}$ in the first Brillouin zone [26] there are three eigenfrequencies $\omega(\boldsymbol{k})$.

Actually, it suffices to consider only half the first Brillouin zone, because the dynamical matrix has the symmetry $\hat{\mathbf{F}}(-\boldsymbol{k}) = -\hat{\mathbf{F}}(\boldsymbol{k})$. The eigenfrequencies for $\pm\boldsymbol{k}$ are related by

$$\omega_1(-\boldsymbol{k}) = -\omega_{-1}^*(\boldsymbol{k}), \quad \omega_0(-\boldsymbol{k}) = -\omega_0(\boldsymbol{k}). \tag{24}$$

It suffices to consider wave vectors $\boldsymbol{k}$ for which $\omega_0(\boldsymbol{k}) \geqslant 0$, since the waves for $-\boldsymbol{k}$ describe the same physical situation as for $\boldsymbol{k}$. We call the wave with frequency $\omega_0(\boldsymbol{k})$ the acoustic wave, since we find that $\omega_0(\boldsymbol{k})$ tends to zero for $\boldsymbol{k} \to \boldsymbol{0}$. For unstable modes the eigenfrequencies $\omega_{\pm 1}(\boldsymbol{k})$ of the optical waves are complex conjugate. We denote the growth rate of unstable waves as $\lambda_1(\boldsymbol{k}) > 0$. One can study the behavior in the limit $\boldsymbol{k} \to \boldsymbol{0}$ in a separate asymptotic analysis keeping only the dominant terms.

It is convenient to use wave vectors $\boldsymbol{q} = \boldsymbol{k}d/2\pi$ and to define components (q_1, q_2, q_3) in terms of the basic vectors of the reciprocal lattice by

$$\boldsymbol{q} = (q_1 \boldsymbol{b}_1 + q_2 \boldsymbol{b}_2 + q_3 \boldsymbol{b}_3) d. \tag{25}$$

Similarly for the vector $\boldsymbol{x} = \boldsymbol{r}/d$ we define components x_1, x_2, x_3 by

$$\boldsymbol{x} = (x_1 \boldsymbol{a}_1 + x_2 \boldsymbol{a}_2 + x_3 \boldsymbol{a}_3)/d. \tag{26}$$

These are related to the cartesian vector components $\boldsymbol{r} = (x,y,z) = (r_1, r_2, r_3)$ by the linear transformation

$$r_\alpha = S_{\alpha\beta} x_\beta, \tag{27}$$

with matrix elements $S_{\alpha\beta} = \boldsymbol{e}_\alpha \cdot \boldsymbol{e}_\beta$. Since the scalar product $\boldsymbol{k} \cdot \boldsymbol{r}$ equals $2\pi \boldsymbol{q} \cdot \boldsymbol{x}$ one has

$$2\pi q_\alpha = S_{\beta\alpha} k_\beta. \tag{28}$$

The Ewald representation used by Nijboer and de Wette [25] reads in present notation

$$S'\left(0 \left| \frac{\boldsymbol{k}}{2\pi}, p\right.\right) = \frac{1}{d^{2p}\Gamma(p)} \left[\sum_{\boldsymbol{n}}{}' \frac{\Gamma(p, \pi \boldsymbol{x}_{\boldsymbol{n}}^2)}{\boldsymbol{x}_{\boldsymbol{n}}^{2p}} \exp(2\pi i \boldsymbol{q} \cdot \boldsymbol{x}_{\boldsymbol{n}}) - \frac{\pi^p}{p} + \frac{\pi^{2p-3/2}}{v_a} \sum_{\boldsymbol{n}} |\boldsymbol{h}_{\boldsymbol{n}} - \boldsymbol{q}|^{2p-3} \times \Gamma\left(-p + \frac{3}{2}, \pi |\boldsymbol{h}_{\boldsymbol{n}} - \boldsymbol{q}|^2\right) \right], \tag{29}$$

where $v_a = \boldsymbol{a}_1 \cdot (\boldsymbol{a}_2 \times \boldsymbol{a}_3)/d^3$ is the dimensionless volume of a unit cell, $\Gamma(p,z)$ is the incomplete gamma function, and $\boldsymbol{h}_{\boldsymbol{n}}$ are the reciprocal lattice vectors

$$\boldsymbol{h}_{\boldsymbol{n}} = (n_1 \boldsymbol{b}_1 + n_2 \boldsymbol{b}_2 + n_3 \boldsymbol{b}_3)/d, \tag{30}$$

where n_1, n_2, n_3 are integers. We need expression (29) for the values $p = \frac{3}{2}$ and $p = \frac{5}{2}$.

The differentiations in Eqs. (21)–(23) can be performed in the Ewald representation of the lattice sums. The required lattice sums can be evaluated straightforwardly for selected wave vectors $\boldsymbol{k}$, provided k is not too small. The dynamical matrix $\hat{\mathbf{F}}(\boldsymbol{k})$ is calculated from the derivatives defined in Eqs. (21)–(23) of the Ewald sum given by Eq. (29). The numerical calculation fails at long wavelengths because of the divergence of the dynamical matrix. Typically the smallest wavenumber considered in the calculation is $k = 0.001 \times 2\pi/d$.

Consider first the simple cubic array with basic vectors $\boldsymbol{a}_1 = (1,0,0)d$, $\boldsymbol{a}_2 = (0,1,0)d$, $\boldsymbol{a}_3 = (0,0,1)d$ and gravity directed along the z axis. We show in the following section that this array is unstable for modes with wave vector $\boldsymbol{k}$ with polar angle θ such that the polynomial

$$A(\theta) = (\sin^2\theta)[1 - 10.7372 \cos^2\theta] \tag{31}$$

is positive. The maximum growth rate for $\theta = \pi/2$ in the limit of small k is $\lim_{k \to 0} \lambda_1(k \cos\varphi, k \sin\varphi, 0) = 2.878\,56 \omega_K$ independent of the direction of $\boldsymbol{k}$ in the horizontal plane. Note that the growth rate does not vanish in the limit $\boldsymbol{k} \to \boldsymbol{0}$, so that the instability is not of the type discussed by Lahiri *et al.* [24] on the basis of macroscopic equations. These authors did not take proper account of the long-range hydrodynamic interaction. In Fig. 1 we plot the growth rate $\lambda_1(\boldsymbol{k})$ for $\boldsymbol{k} = (k,0,0)$. The corresponding eigenvector has components in the x and z directions. The third mode has vanishing eigenfrequency and eigenvector in the y direction.

Next we consider a body-centered cubic array with basic vectors [26] $\boldsymbol{a}_1 = (1,1,-1)d/2$, $\boldsymbol{a}_2 = (-1,1,1)d/2$, $\boldsymbol{a}_3 = (1,-1,1)d/2$ and gravity directed along $\boldsymbol{a}_3$. We define polar angles (θ,φ) of the unit vector $\hat{\boldsymbol{k}} = \boldsymbol{k}/k$ by

$$\hat{\boldsymbol{k}} = \hat{\boldsymbol{a}}_3 \cos\theta + \hat{\boldsymbol{b}}_1 \sin\theta \cos\varphi + \hat{\boldsymbol{a}}_3 \times \hat{\boldsymbol{b}}_1 \sin\theta \sin\varphi, \tag{32}$$

with reciprocal lattice vector $\boldsymbol{b}_1 = (1,1,0)/d$. The array is unstable for modes with wave vector $\boldsymbol{k}$ of small wave number k and with direction (θ,φ) such that the polynomial

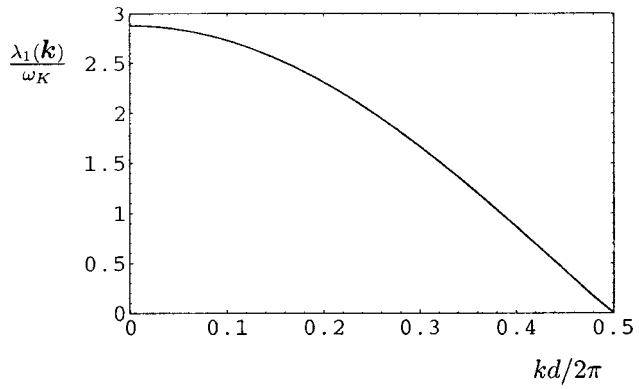

FIG. 1. Plot of the growth rate $\lambda_1(\boldsymbol{k})$ for $\boldsymbol{k}=(k,0,0)$ for the simple cubic array with gravity directed along the z axis. The basic lattice vectors are $\boldsymbol{a}_1=(1,0,0)d$, $\boldsymbol{a}_2=(0,1,0)d$, $\boldsymbol{a}_3=(0,0,1)d$.

$$A(\theta,\varphi)=\sin^2\theta[1-2.8539\sin^2\theta\cos^2\theta + 1.0090\sin^3\theta\cos\theta\sin 3\varphi] \tag{33}$$

is positive. The growth rate is maximal for direction $(\theta_0,\varphi_0)=(0.7088,\pi/2)$, as well as for $(\theta_0,7\pi/6)$ and $(\theta_0,11\pi/6)$, and then takes the value $\lambda_1=5.8016\omega_K$. The eigenfrequencies vary rapidly with k for small k. We find that the eigenfrequencies are real except for small k. In particular, for direction (θ_0,φ_0) the eigenfrequencies are real for $k>0.000\,15\times 2\pi/d$. Hence the bcc array is mesoscopically stable. In Fig. 2 we plot the phase velocity $\omega_0(\boldsymbol{k})/k$ for $k=0.001\times 2\pi/d$ as a function of direction for $\theta<\pi/2$. The other part of the surface follows by reflection with respect to the origin. In Fig. 3 we plot the three dispersion curves for $\omega_{\pm 1}(\boldsymbol{k}),\omega_0(\boldsymbol{k})$ as functions of wave number in the first Brillouin zone for direction $(1,1,1)/\sqrt{3}$. Typically the two larger eigenfrequencies $\omega_{\pm 1}(\boldsymbol{k})$ differ significantly from the lower one. The sum of the three eigenfrequencies is always close to zero. We find numerically that the eigenvector corresponding to $\omega_0(\boldsymbol{k})$ is predominantly transverse, also for other directions of $\boldsymbol{k}$.

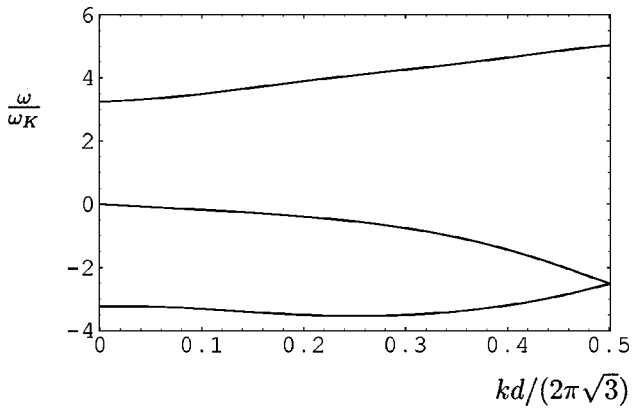

FIG. 3. Plot of the eigenfrequencies $\omega_{-1}(\boldsymbol{k}),\omega_0(\boldsymbol{k})$, and $\omega_1(\boldsymbol{k})$ (bottom to top) as functions of wave number k for direction $\hat{\boldsymbol{k}}=(1,1,1)/\sqrt{3}$ for the bcc array as described in the caption to Fig. 2.

Finally we consider the face-centered cubic array with basic vectors [26] $\boldsymbol{a}_1=(1,1,0)d/2$, $\boldsymbol{a}_2=(0,1,1)d/2$, $\boldsymbol{a}_3=(1,0,1)d/2$ and gravity directed along $\boldsymbol{a}_3$. This array is also mesoscopically stable. The asymptotic analysis of the following section shows that the frequencies $\omega_{\pm 1}(\boldsymbol{k})$ become complex for very small $\boldsymbol{k}$ for directions θ,φ such that an angle polynomial $A(\theta,\varphi)$ is positive. In this case the polynomial is a sum of products of $\cos\theta$,$\sin\theta$,$\cos\varphi$,$\sin\varphi$ consisting of 12 terms with coefficients calculated from lattice sums. The polynomial is positive in four regions on the unit sphere, related by reflection. The growth rate is maximal for direction $(\theta_0,\varphi_0)=(0.3463,0.9553)$ and its inverse, and given by $\lim_{k_0\to 0}\lambda_1(\boldsymbol{k}_0)=5.2887\omega_K$. For this direction the eigenfrequencies are real for $k>0.000\,17\times 2\pi/d$.

In Fig. 4 we plot the phase velocity $\omega_0(\boldsymbol{k})/k$ for $k=0.001\times 2\pi/d$ as a function of direction for $\theta<\pi/2$. Polar angles are defined as in Eq. (32) with reciprocal lattice vector $\boldsymbol{b}_1=(1,1,-1)/d$. The other part of the surface follows by reflection with respect to the origin. In directions perpendicu-

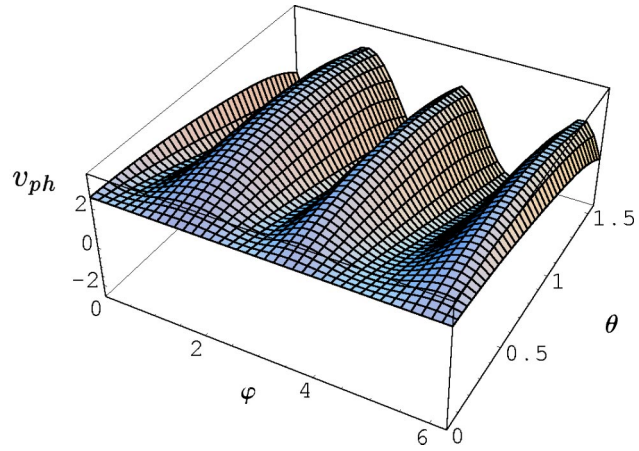

FIG. 2. Plot of the phase velocity $\omega_0(\boldsymbol{k})/k$ in units $\omega_K d/2\pi$ for $k=0.001\times 2\pi/d$ for the body-centered cubic array with basic vectors $\boldsymbol{a}_1=(1,1,-1)d/2$, $\boldsymbol{a}_2=(-1,1,1)d/2$, $\boldsymbol{a}_3=(1,-1,1)d/2$ and gravity directed along $\boldsymbol{a}_3$. The phase velocity is plotted for the range of directions $0<\theta<\pi/2$, $0<\varphi<2\pi$.

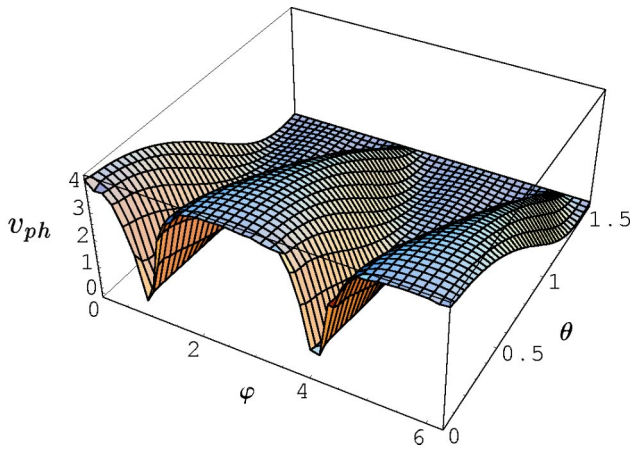

FIG. 4. Plot of the phase velocity $\omega_0(\boldsymbol{k})/k$ for $k=0.001\times 2\pi/d$ for the face-centered cubic array with basic vectors $\boldsymbol{a}_1=(1,1,0)d/2$, $\boldsymbol{a}_2=(0,1,1)d/2$, $\boldsymbol{a}_3=(1,0,1)d/2$ and gravity directed along $\boldsymbol{a}_3$. The phase velocity is plotted for the range of directions $0<\theta<\pi/2$, $0<\varphi<2\pi$.

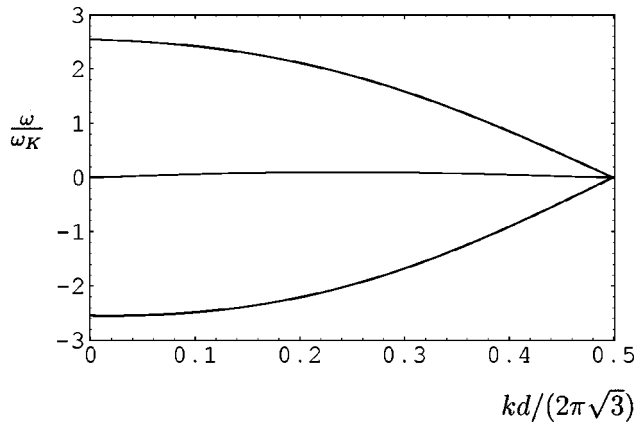

FIG. 5. Plot of the eigenfrequencies $\omega_{-1}(\boldsymbol{k}),\omega_0(\boldsymbol{k})$, and $\omega_1(\boldsymbol{k})$ (bottom to top) as functions of wave number k for direction $\hat{\boldsymbol{k}}=(1,1,1)/\sqrt{3}$ for the fcc array as described in the caption to Fig. 4.

lar to gravity the frequency $\omega_0(\boldsymbol{k})$ is vanishingly small for all values of the wave number. The plot differs significantly from the corresponding plot for the bcc array shown in Fig. 2. As one would expect, the crystal structure has a strong influence on the shape of the dispersion surface. In Fig. 5 we plot the three real eigenfrequencies as functions of wave number for direction $(1,1,1)/\sqrt{3}$. The sum of the three eigenfrequencies is always close to zero. We find numerically that the eigenvector corresponding to $\omega_0(\boldsymbol{k})$ is predominantly transverse, also for other directions of $\boldsymbol{k}$.

For other directions of the gravity field the fcc array becomes more unstable. As an example we show in Fig. 6 the variation of $-\mathrm{Re}[\omega_{-1}(\boldsymbol{k})]$ and the growth rate $\lambda_1(\boldsymbol{k})$ for wave vector $\boldsymbol{k}=0.001[\sin(\pi/8),0,\cos(\pi/8)]2\pi/d$ as the direction of gravity changes from $(1,0,1)/\sqrt{2}$ to $(0,0,1)$ in the plane spanned by these two vectors. This shows that the orientation of the lattice with respect to gravity is quite relevant.

In periodic boundary conditions the mesoscopically stable arrays are stable for system size less than a maximum value. The sedimentation waves found above for such stable arrays are interesting, since we are dealing with a purely dissipative

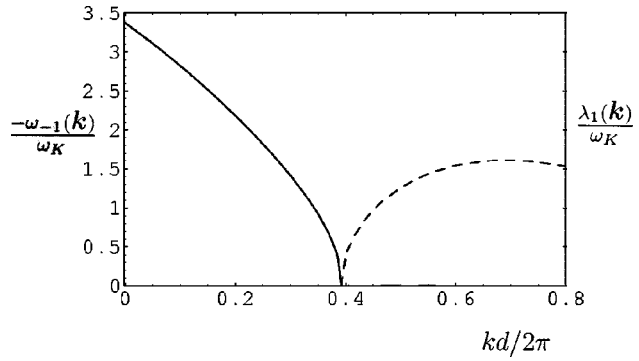

FIG. 6. Plot of frequency $-\mathrm{Re}[\omega_{-1}(\boldsymbol{k})]$ (solid curve) and growth rate $\lambda_1(\boldsymbol{k})$ (dashed curve) for the fcc array for wave vector $\boldsymbol{k}=0.001[\sin\pi/8,0,\cos(\pi/8)]2\pi/d$ as the direction of gravity changes from $(1,0,1)/\sqrt{2}$ to $(0,0,1)$ in the plane spanned by these vectors.

system. The structure of the three modes for each wave vector is determined by lattice symmetry and direction of the gravitational field. The frequency of each mode is proportional to the strength of the field. In a recent experiment [27] spheres of radius $a=1.5\times10^{-2}$ cm and mass density $\rho_p=4.11$ g/cm^3 in a fluid of shear viscosity $\eta=10$ P and mass density $\rho_f=0.965$ g/cm^3 were used. With gravitational acceleration $g=983$ cm/sec^2 and interparticle distance $d=0.1$ cm this corresponds to a characteristic frequency $\omega_K=0.017$ s^{-1}. Dispersion curves of sedimentation waves have not yet been studied experimentally.

IV. LONG-WAVELENGTH LIMIT

As noted above, the dynamical matrix $\hat{\mathbf{F}}(\boldsymbol{k})$ diverges in the small k limit due to the long range of the hydrodynamic interaction. We must study the limiting behavior by asymptotic analysis keeping only the dominant terms. The analysis makes clear that the limiting behavior depends on the direction of the wave vector with respect to the crystal axes. In this section we present explicit results for the three cubic arrays with gravity directed along the basic vector $\boldsymbol{a}_3$.

The term $\boldsymbol{n}=\mathbf{0}$ in the second sum in Eq. (29) for $p=\frac{3}{2}$ yields a logarithmic singularity for small $\boldsymbol{k}$, since

$$\Gamma(0,z)=E_1(z) \tag{34}$$

and the exponential integral $E_1(z)$ has the expansion [28]

$$E_1(z)=-\gamma-\ln z-\sum_{n=1}^{\infty}\frac{(-1)^n z^n}{nn!}\quad(|\arg z|<\pi), \tag{35}$$

where γ is Euler's constant. The function $\Gamma(-1,z)$ corresponding to $p=\frac{5}{2}$ is given by

$$\Gamma(-1,z)=\frac{e^{-z}}{z}-\Gamma(0,z). \tag{36}$$

The stronger singularity is compensated by the factor multiplying the Γ function in Eq. (29). Performing the derivatives in Eqs. (21)–(23) we find that the singular behavior of the tensor $\hat{\mathbf{F}}(\boldsymbol{k})$ for $\boldsymbol{k}\to\mathbf{0}$ takes the form

$$\hat{F}_{\alpha\beta}(\boldsymbol{k},\hat{\boldsymbol{K}})=\frac{1}{k^4 d}\sum_{\gamma\delta}C_{\alpha\beta\gamma\delta}k_\alpha k_\beta k_\gamma\hat{K}_\delta+O(1), \tag{37}$$

with numerical coefficients $C_{\alpha\beta\gamma\delta}$ depending on lattice structure. In order to find the coefficients we need to expand $S'(0|(\boldsymbol{k}/2\pi),\frac{3}{2})$ to quadratic order in the components of $\boldsymbol{k}$, and $S'(0|(\boldsymbol{k}/2\pi),\frac{5}{2})$ to quartic order. Thus we write

$$S'\left(0\left|\frac{\boldsymbol{k}}{2\pi},p\right.\right)=\frac{1}{d^{2p}\Gamma(p)}\left[\frac{\pi^{2p-3/2}}{v_a}\boldsymbol{q}^{2p-3}\Gamma\left(-p+\frac{3}{2},\pi\boldsymbol{q}^2\right)\right.$$
$$+R_0(p)+\frac{1}{2}R^{(2)}_{ij}(p)q_iq_j$$
$$\left.+\frac{1}{24}R^{(4)}_{ijkl}(p)q_iq_jq_kq_l\right]+O(k^6). \tag{38}$$

Due to invariance under reflections there are no terms odd in $\boldsymbol{q}$. The coefficients R follow by expansion in Eq. (29). For the cubic lattices one can use symmetry considerations to reduce the number of coefficients that need to be calculated.

The characteristic equation

$$\det[\hat{\omega}\mathbf{1}-\hat{\mathbf{F}}(\boldsymbol{k})]=0, \tag{39}$$

which yields the eigenfrequencies is a cubic in $\hat{\omega}=\omega/\omega_K$ that takes the form

$$\hat{\omega}^3+c_2\hat{\omega}^2+c_1\hat{\omega}+c_0=0, \tag{40}$$

with dimensionless coefficients c_0,c_1,c_2. It turns out that for the cubic arrays the coefficients remain finite in the limit $\boldsymbol{k}\to\mathbf{0}$, though the limiting behavior depends on the direction in which the origin of $\boldsymbol{k}$ space is approached. The coefficients c_0 and c_2 vanish as $\boldsymbol{k}\to\mathbf{0}$, whereas the coefficient c_1 tends to a nonvanishing constant. As a consequence the roots $\hat{\omega}_{\pm1}(\boldsymbol{k})$ tend to

$$\hat{\omega}^{(0)}_{\pm1}(\theta,\varphi)=\pm\sqrt{-c^{(0)}_1(\theta,\varphi)}, \tag{41}$$

where $c^{(0)}_1(\theta,\phi)$ gives the angular dependence of the coefficient $c_1(\boldsymbol{k})$ in the limit $\boldsymbol{k}\to\mathbf{0}$. The root $\hat{\omega}_0(\boldsymbol{k})$ tends to

$$\hat{\omega}^{(1)}_0(\theta,\varphi)=-\frac{c^{(1)}_0(\theta,\varphi)}{c^{(0)}_1(\theta,\varphi)}\frac{kd}{2\pi}, \tag{42}$$

where $c^{(1)}_0(\theta,\varphi)k$ gives the limiting behavior of the coefficient $c_0(\boldsymbol{k})$ for small $\boldsymbol{k}$.

The stability of the array is determined by the sign of the coefficient $c^{(0)}_1(\theta,\varphi)$. For each of the cubic lattices we find a domain of angles for which the coefficient is positive, so that these arrays are unstable. The phase velocity of the acoustic wave tends to

$$v_{ph}(\theta,\varphi)=-\frac{c^{(1)}_0(\theta,\varphi)}{c^{(0)}_1(\theta,\varphi)}\frac{\omega_Kd}{2\pi} \tag{43}$$

in the limit of small $\boldsymbol{k}$. This diverges for angles where $c^{(0)}_1(\theta,\varphi)$ changes sign.

The functions $c^{(0)}_1(\theta,\varphi)$ and $c^{(1)}_0(\theta,\varphi)$ can be evaluated explicitly in terms of sums of products of trigonometric functions with coefficients given by Ewald sums. For the simple cubic lattice with basic vectors as defined above Eq. (31) and with gravity directed along the z-axis one finds for the function $c^{(0)}_1(\theta,\varphi)$

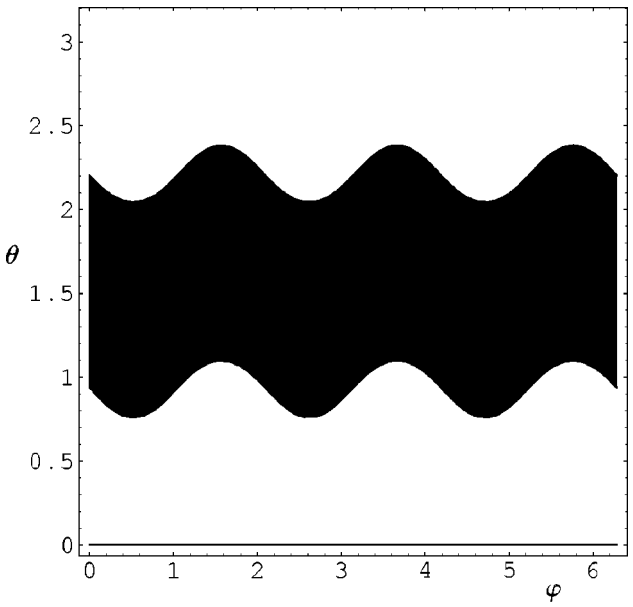

FIG. 7. The white region is the domain of directions on the unit sphere for which the bcc array is unstable in the long-wavelength limit.

$$c^{(0)}_1(\theta,\varphi)=\sin^2\theta[8.2861-88.9699\cos^2\theta]. \tag{44}$$

The polar angles are defined as in Eq. (32) with the above basic vectors and reciprocal vector $\boldsymbol{b}_1=(1,0,0)/d$. The function is positive for $1.4475<\theta<1.6641$. The maximum growth rate is for $\theta=\pi/2$ and takes the value

$$\lim_{k\to0}\lambda_1(k\cos\varphi,k\sin\varphi,0)=2.878\,56\omega_K \tag{45}$$

independent of the direction of $\boldsymbol{k}$ in the horizontal plane. For the function $c^{(1)}_0(\theta,\varphi)$ one finds

$$c^{(1)}_0(\theta,\varphi)=\sin^2\theta[17.165\cos\theta-184.304\cos^3\theta], \tag{46}$$

showing that the limiting value of the phase velocity of the acoustic wave is independent of the azimuthal angle φ.

For the bcc array, as defined at the end of the preceding section, one finds for the function $c^{(0)}_1(\theta,\varphi)$

$$c^{(0)}_1(\theta,\varphi)=\sin^2\theta[-69.4836+198.3000\cos^2\theta$$
$$-70.1095\sin\theta\cos\theta\sin3\varphi], \tag{47}$$

In Fig. 7 we plot the region of the (θ,φ) plane, where this function is positive, and hence the array is unstable. In Fig. 8 we plot the function $c^{(0)}_1(\theta,\varphi)$ itself. The growth rate is maximal for direction $(\theta_0,\varphi_0)=(0.7088,\pi/2)$, as well as for $(\theta_0,7\pi/6)$ and $(\theta_0,11\pi/6)$, and then takes the value $\lambda_1=5.8016\omega_K$. For the function $c^{(1)}_0(\theta,\varphi)$ one finds

$$c^{(1)}_0(\theta,\varphi)=-1291.91r^3s^2+1406.33rs^4$$
$$+703.135s^5v(4u^2-1)$$
$$-600.412r^2s^3v(4u^2-1), \tag{48}$$

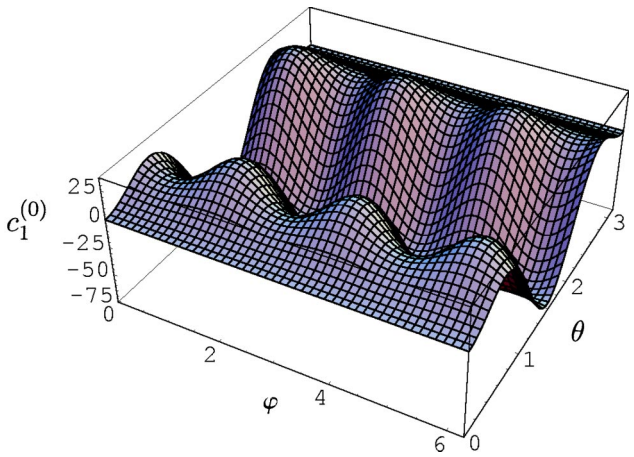

FIG. 8. Plot of the function $c_1^{(0)}(\theta,\varphi)$ for the bcc array, as given by Eq. (47). The array is unstable where the function is positive.

with the abbreviations $r=\cos\theta$, $s=\sin\theta$, $u=\cos\varphi$, $v=\sin\varphi$.

For the face-centered cubic array with basic vectors as defined above and with gravity directed along $\boldsymbol{a}_3$ one finds for the function $c_1^{(0)}(\theta,\varphi)$,

$$\begin{aligned} c_1^{(0)}(\theta,\varphi) = {} & 66.76rsu(1-2s^2-s^2u^2)-62.62r^2s^2-84.42s^4 \\ & -100.91r^2s^2u^2+50.45s^4u^2+94.41r^3sv \\ & +285.41r^2s^2uv-142.71s^4uv-151.05rs^3u^2v \\ & -169.93rs^2v^3, \end{aligned} \tag{49}$$

where the angles are defined as in Eq. (32) with the above basic vectors and with reciprocal lattice vector $\boldsymbol{b}_1=(1,1,-1)/d$. In Fig. 9 we plot the region of the (θ,φ) plane, where this function is positive, and hence the array is unstable. In Fig. 10 we plot the function $c_1^{(0)}(\theta,\varphi)$ itself. The

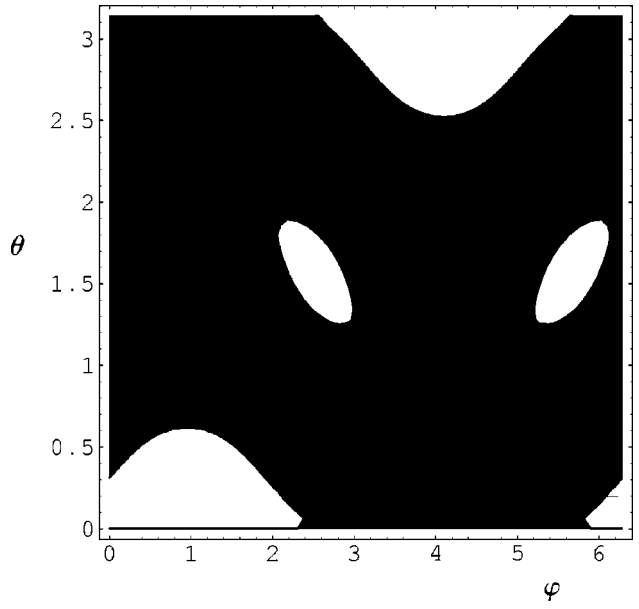

FIG. 9. The white region is the domain of directions on the unit sphere for which the fcc array is unstable in the long wavelength limit.

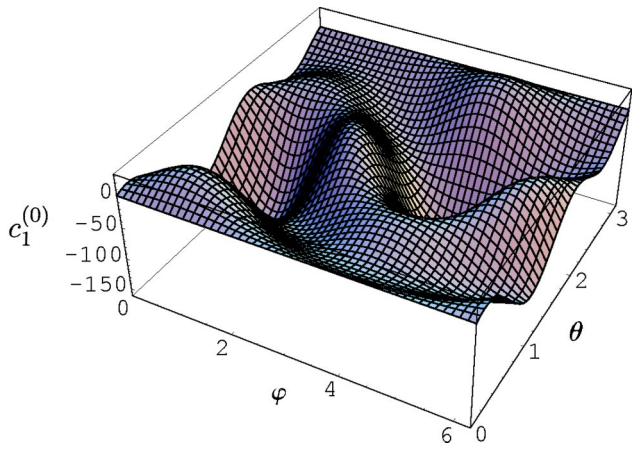

FIG. 10. Plot of the function $c_1^{(0)}(\theta,\varphi)$ for the fcc array, as given by Eq. (49). The array is unstable where the function is positive.

growth rate is maximal for direction $(\theta_0,\varphi_0)=(0.3463,0.9553)$ and its inverse, and given by $\lim_{k_0\to 0}\lambda_1(\boldsymbol{k}_0)=5.2887\omega_K$. For the function $c_0^{(1)}(\theta,\varphi)$ one finds

$$\begin{aligned} c_0^{(1)}(\theta,\varphi) = {} & 97.27r^4su+1306.24r^3s^2u^2-230.14r^2s^3u^3 \\ & -474.97rs^4u^4-12.58s^5u^5+137.56r^4sv \\ & -1657.00r^3s^2uv-198.79r^2s^3u^2v \\ & -611.65rs^4u^3v-75.03s^5u^4v+720.40r^3s^2v^2 \\ & -6.20r^2s^3uv^2+3.62rs^4u^2v^2-126.35s^5u^3v^2 \\ & -262.13r^2s^3v^3+215.52rs^4uv^3-121.44s^5u^2v^3 \\ & -544.99rs^4v^4-113.78s^5uv^4-46.41s^5v^5. \end{aligned} \tag{50}$$

These asymptotic results suggest that the fcc array is the most stable configuration of the three cubic arrays with gravity directed along one of the basic vectors.

V. DISCUSSION

Direct numerical evaluation of the characteristic equation, as presented in Sec. III for the bcc array, suggests that both the bcc array and the fcc array with gravity directed along one of the basic vectors are stable. For very small k direct numerical evaluation is not feasible, since the elements of the dynamical matrix diverge with the inverse power of wave number. The asymptotic calculation, studied in Sec. IV, yields exact results for the $\boldsymbol{k}\to\boldsymbol{0}$ limit, and shows that in fact the arrays are not stable. It is difficult to close the gap between the two regimes of very long and intermediate wavelengths. From the disparity of results we can conclude only that the eigenfrequencies must vary rapidly in the gap. Nonetheless, the numerical evaluation for nonvanishing k shows only propagating modes. This indicates that the arrays are stable in periodic boundary conditions up to a maximum system size corresponding to the minimum wave number

beyond which all modes are stable. For the bcc array we find that in the direction of maximum growth the eigenfrequencies are real for $k>0.000\,15\times 2\pi/d$. For the fcc array the eigenfrequencies are real for $k>0.000\,17\times 2\pi/d$ for the direction of maximum growth. We therefore call these arrays mesoscopically stable.

The existence of stable settling arrays with small fluctuations in particle velocity is important for the theory of sedimentation. As mentioned earlier, theory and numerical computations with randomly positioned particles lead to particle velocity fluctuations that diverge with the size of the system [11–13]. For mesoscopically stable arrays the particle velocities are small and the microstructure remains close to the regular lattice configuration. Macroscopic instability may be prevented by a limitation on the size of the system. Particle swirls seen in experiment [29] may possibly be understood as sedimentation waves.

The calculations can be extended in various ways. The calculation for long wavelengths of Sec. IV in principle can be carried out to next order in wave number. This would exhibit the limiting behavior in more detail. It would also be of interest to vary the direction of gravity with respect to the crystal axes, and to investigate how this affects the instability at long wavelengths. Finally, it would be of interest to extend the calculation to higher order in density. This would be a challenging task, since it would require inclusion of higher order force multipoles and an arbitrary number of reflections between particles. Nonetheless, the periodicity of the array can be exploited.

Now that the concept of mesoscopic stability has been established for periodic arrays it would be of interest to explore the stability of disordered arrays along the same lines. Conceivably, a disordered microstructure can be constructed that yields stability at short and intermediate wavelengths, even though it fails on the macroscopic scale.

Finally, it would be of interest to study the vibrations of particles about their lattice positions in finite stable arrays from a statistical point of view. This would require a decomposition of the vibrations in sedimentation waves, and a postulated statistical distribution of wave amplitudes.

[1] H. Hasimoto, J. Fluid Mech. **5**, 317 (1959).
[2] A.A. Zick and G.M. Homsy, J. Fluid Mech. **115**, 13 (1982).
[3] A.S. Sangani and A. Acrivos, Int. J. Multiphase Flow **8**, 343 (1982).
[4] G.K. Batchelor, J. Fluid Mech. **52**, 245 (1972).
[5] J.F. Brady and L.J. Durlofsky, Phys. Fluids **31**, 717 (1987).
[6] B. Cichocki and B.U. Felderhof, Physica A **154**, 213 (1989).
[7] R.H. Davis and A. Acrivos, Annu. Rev. Fluid Mech. **17**, 17 (1985).
[8] E. J. Hinch, in *Disorder and Mixing*, edited by E. Guyon *et al.* (Kluwer, Dordrecht, 1988), p. 153.
[9] R. Blanc and E. Guyon, Recherche **22**, 866 (1991).
[10] S. Ramaswamy, Adv. Phys. **50**, 297 (2001).
[11] R.E. Caflisch and J.H.C. Luke, Phys. Fluids **28**, 759 (1985).
[12] A.J.C. Ladd, Phys. Fluids **9**, 491 (1997).
[13] D.L. Koch and E.S.G. Shaqfeh, J. Fluid Mech. **224**, 275 (1991).
[14] H. Nicolai and E. Guazzelli, Phys. Fluids **7**, 3 (1995).
[15] A. Levine, S. Ramaswamy, E. Frey, and R. Bruinsma, Phys. Rev. Lett. **81**, 5944 (1998).
[16] P. Tong and B.J. Ackerson, Phys. Rev. E **58**, R6 931 (1998).
[17] M.P. Brenner, Phys. Fluids **11**, 754 (1999).
[18] J.H.C. Luke, Phys. Fluids **12**, 1619 (2000).
[19] A.J.C. Ladd, Phys. Rev. Lett. **88**, 048301 (2002).
[20] J.M. Crowley, J. Fluid Mech. **45**, 151 (1971).
[21] J.M. Crowley, Phys. Fluids **19**, 1296 (1976).
[22] M.A. Rutgers, J.-Z. Xue, E. Herbolzheimer, W.B. Russel, and P.M. Chaikin, Phys. Rev. E **51**, 4674 (1995).
[23] R. Lahiri and S. Ramaswamy, Phys. Rev. Lett. **79**, 1150 (1997).
[24] R. Lahiri, M. Barma, and S. Ramaswamy, Phys. Rev. E **61**, 1648 (2000).
[25] B.R.A. Nijboer and F.W. de Wette, Physica (Amsterdam) **23**, 309 (1957).
[26] C. Kittel, *Introduction to Solid State Physics* (Wiley, New York, 1996).
[27] L. Bergougnoux, S. Ghicini, É. Guazzelli, and J. Hinch, Phys. Fluids **15**, 1875 (2003).
[28] M. Abramowitz and I. A. Stegun, *Handbook of Mathematical Functions* (Dover, New York, 1965).
[29] P.N. Segré, E. Herbolzheimer, and P.M. Chaikin, Phys. Rev. Lett. **79**, 2574 (1997).